Proceedings of the 2019 IEEE/ASME
International Conference on Advanced Intelligent Mechatronics
Hong Kong, China, July 8-12, 2019

Three-dimensional Localization of Needle Tip Immersed in Medium

Zhenxi Cui, Kaicheng Huang, Bo Lu, and Henry K. Chu*, Member, IEEE

***Abstract*— Pick and place through micro manipulators has been an indispensable tool for a variety of biomedical applications. In tissue engineering, 3D tissue can be fabricated through the stacking of multiple cells sheets together. To enable precise handling and alignment of cell sheets, accurate detection of a probe tip, which could experience wave distortion from the culture medium during tip manipulation is very important. In this paper, the 3D position of a tip is evaluated using a vision system. Based on 2D images from consecutive frames, the kernel describing the effect from motion is first computed using a motion blur model. Then, an auto regressive (AR) method is employed to extract the scale factor corresponded to the depth of Z coordinate. Parameters in the model are recursively updated using Unscented Kalman Filter (UKF) algorithm. By finding the tip position in the 2D image, its depth information can be found accordingly. Experiments were conducted to examine the performance and accuracy in evaluating the position of a tip immersed in an aqueous environment.**

I. Introduction

In tissue engineering, the technique to construct 3D tissues in vitro has received increasing attention from researchers. In the field, one of the methods is to assemble cells into 3D clusters through the use of scaffold and other tools [1] [2] [3]. In this process, a temporary mould or scaffold is needed to be fabricated, and different designs are required for different types of cells. Considering the complexity of 3D human tissues, this method is inevitably time-consuming and technology expensive. Another stream of the research is to pattern cells on a biocompatible hydrogel, and the formed cell sheets are stacked together into 3D using a manipulator equipped with a gripper or pipette. With the inherited advantages of high flexibility and precision, micro-manipulators have also been implemented in many operations such as cell injection, cell sheet grasping, and cell separation. Automation of cell stacking has also been in a great process [4] [5].

Nowadays, many advanced manipulators and microscopes have already been developed, Nevertheless, there are still many issues related to the use of manipulators. As a contact-based method, the interaction between the cell sheet and the end-effector tip is an important part. Both the fragility of hydrogels and the applied force between the cells and the gripper tip bring challenges on continuous and stable manipulation. Also, maintaining an optimal enviroment is essential for cells to grow, including controlled temperature, suitable substrate for cell attachment, and appropriate cell culture medium with proper pH value and osmolality. When veiwing the semi-transparent cell-laden sheet under the microscope, images could be distorted or degraded by the culture medium. Besides, the wave or ripple phenomenon [6] excited by the motion of the manipulator is another obstacle for localizing the tip which is important but has not been explored extensively. Normally, the distortion caused by the refraction is apparent in a static underwater scenario. Much attention has been paid to the restoration of the original image [7] [8]. However, the skew and blur problems caused by the manipulator's motion under the cell culture medium is large, resulting in difficult tip localization with huge bias, even in 2D (X, Y) plane. Fig. 1 gives an illustration of skew and blur when the ripple causes the microscope's image with large degradation. Not only the X and Y coordinates on the image plane is unclear, but also along the optical axis which is an inherent problem in the 2D microscope environment. All the above mentioned problems should be carefully considered before the cell sheet stacking and handling operations can be proceeded.

(a) Manipulator tip (b) Motion blurred tip

Fig. 1: The blur problem in the cell culture medium

To solve the aforementioned problems, we relate the effect of motion blur through image analysis. In this context, we proposed a method which can be implemented to locate the manipulator tip immersed in the cell culture medium. The outline of the paper is as follows: firstly, related work on the localization of the end-effector tip and image de-blurring techniques in a liquid environment is reviewed. Then the problem is formulated and the proposed depth evaluation based on motion blur is introduced. After that, experiments to validate the proposed model are discussed. Finally, a conclusion is given to summarize the finding.

In a microscope-based probe or gripper manipulation, continuous tip (X, Y, Z) coordinates are needed for visual monitoring and control. Much work has been done for perceiving the 3D tip coordinates [9] [10] [11] [12], so as to make the micromanipulation, such as alignment and

The work was supported in part by the Research Grant Council of the Hong Kong Special Administrative Region, China, under Grant 25204016.

Z. Cui, K. Huang, Bo Lu and H. K. Chu are with the Department of Mechanical Engineering, The Hong Kong Polytechnic University, Hong Kong. (* Corresponding Author, email: henry.chu@ polyu.edu.hk)

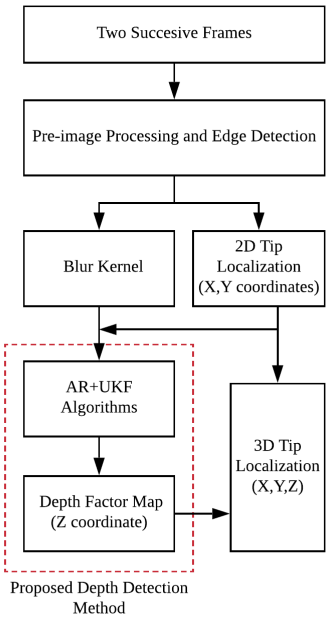

Fig. 2: Flow chart of the method

pick-and-place, to become more reliable. Gurtner et al. [13] proposed to measure the 3D using a twin-beam position estimation method. Shuai et al. proposed integrating the features detected from the tip surface and the Kalman Filter to help detect the tip location [14]. For 2D ultrasound images, Kaya et al. [15] developed a Gabor filter model to localize the needle tip. Similarly, Ni et al. [16] used an auxiliary vision sensor to position the manipulator's tip. However, all these methods need additional hardware or features to facilitate the evaluation, requiring modifications to a standard microscope equipment. Other approaches such as particle filter model and feature enhancement by probability motion model have also been developed to estimate the tip motion in 2D plane. However, the information in the Z coordinate, or the out-of-plane direction, still may not be accurately predicted. In the process of 3D stacking and alignment, the tips are used to lift up the cell sheets and place on top of another layer of cell sheets. Hence, accurate information of the Z coordinate is as important as the X, Y coordinates. Among the recent work, Jun et al. [4] combined the motion history image (MHI) and focus metrics to get the 3D manipulator tip position, with an assumption that the tip at the end-effector is always mounted with a downward tilting angle, which is not always true. Later, based on the work of [4], Seongsik et al. [17] fitted a linear model between the focus measure and the depth to confirm the depth information. In addition, they compared the proposed model with a support vector machine (SVM) model through experiments. However, the inverse parabolic relationship between focus measure and depth make continuous tracking of the manipulator in 2D become difficult. Also, it is possible that the model could give the wrong direction as it is difficult to distinguish images between under and the above the focal plane [18].

In this paper, we aim to resolve the challenge described in [4][17] for tip localization in a 2D plane (X, Y). In addition, a new vertical estimation model is proposed, which has high reliability and stability. We utilize the motion blur metrics and the UKF model to predict the depth information. This method is a recursive approach that only depends on the low order neighbours, reducing the time in computation. The flow of the proposed method is illustrated in Fig. 2.

II. Problem Formulation and Proposed Method

The hardware used for the experiments is shown in Fig. 3. The system consists of a Stereo Microscope XPZ+V10 mounted with two E3CMOS06300KPA Camera, a Sutter MP-285 (Sutter Instrument, CA, USA) micromanipulator with 3 DOFs. A needle probe is attached to the manipulator to facilitate tip manipulation under the cell culture medium. The algorithm is coded with C++ and MATLAB R2015b (MathWorks Inc., MA, USA). Continuous images with blur are captured from the camera with a resolution of 400×400 pixels. The entire system is placed on an active anti-vibration table to prevent interference from the surrounding.

A. 2D Tip Localization

When the input images are heavily blurred, conventional image processing techniques such as contour detection, image segmentation and object recognition are greatly deteriorated by noises and outliers. Even with the deconvolution techniques, such as Wiener deconvolution, Richardson–Lucy deconvolution [17], these influence can only be alleviated to some degree. In this paper, a two-stage method is implemented to localize the X and Y coordinates of the tip from the blurred images. First, all line segments were detected using the Canny edge detection algorithm. A threshold parameter θ, which is the maximum the allowable angle between two edges was set to filter outline segments which have a huge deviation from the rest of the group. Then, a parabolic line is fitted to represent the contour of the probe. For line segments that are far from the fitted line are treated as outliers. Finally, any remaining line segments are considered as the edge of the probe, as shown in blue in Fig. 5 (a). In the second stage, a white line that is particular to probe central axis in cyan is evaluated. By finding the intersection between the white and cyan line, the tip coordinates in X,Y will be measured and its corresponding depth information will be obtained using a motion blur model.

B. Motion Blur Model

When the micromanipulator is manipulated continuously, the motion blur caused by circular waves or ripples [19], is captured on consecutive microscope video frames. A point spread function (PSF) could be used to resemble the whole frame, except that every single pixel in the frame has a different scale factor to this PSF. The scale factor is a deterministic value related to the depth of each pixel point. Based on that, the blurred image g can be an analogy to one kind of motion blur, and the blur of the pixel point in image g follows a monotonically decreasing function. Let f and h be the original image and the PSF, respectively. The blur model can be modeled [20] [21] as

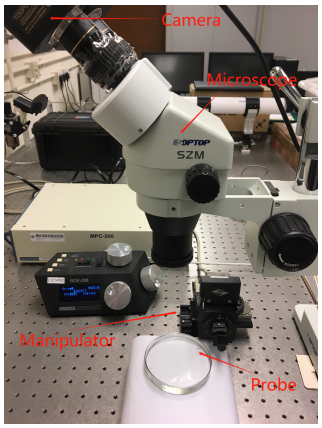

(a) Image of the setup

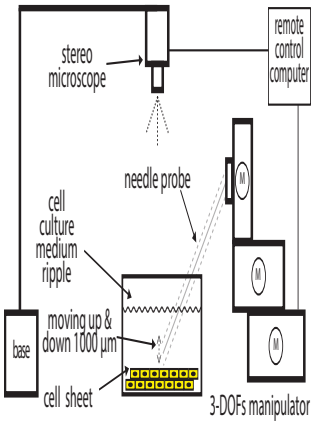

(b) Schematic Diagram

Fig. 3: System configuration

$$f *_v h(x,y) = \int\int f(x-s, y-t)h(x-s, y-t; s, t)dsdt \quad (1)$$

where $*_v$ denotes a space variant blurring kernel. Taking the noisy term e with zero mean and variance σ, into consideration, the blurred image g can be modeled as

$$g(x,y) = f *_v h(x,y) + e(x,y) \quad (2)$$

If a reference anchor point (o_x, o_y) with its depth $d(o_x, o_y)$, and the corresponding PSF $h_0(o_x, o_y; s, t)$ are confirmed in the blurred image g, then the PSF of an arbitrary pixel point (x, y) is a scaled version of the reference PSF , $h_0(o_x, o_y; s, t)$. The model can be given by

$$h(x, y; s, t) = k(x, y)h_0(o_x, o_y; s, t) \quad (3)$$

where $k(x,y) = \frac{d(x,y)}{d_0}$ is the scale factor, a depth ratio between depth $d(x, y)$ at point (x, y) and the benchmark depth d_0 at point (o_x, o_y). Rearranging the equations (1) (2) into scalar form yield

$$f *_v h(m,n) = \sum_{m,n} f(m-x, n-y)h(m-x, n-y; x, y) \quad (4)$$

$$g(x,y) = f *_v h(m,n) + e(x,y) \quad (5)$$

In summary, the observed blurred image $g(x, y)$ is the resultant of a space variant kernel filter $h(x, y)$ applied on the original microscope captured image f, as expressed using equation (4). Let $g_1(x, y)$ and $g_2(x, y)$ denote two consecutive video frames, with $g_1(x, y)$ as the reference image and $g_2(x, y)$ as the observation image. Then this 3D coordinate estimation of the micro tip, or more specifically, the depth can be formulated as

$$g_2(x,y) = g_1(x,y) *_v h(x,y) + e(x,y) \quad (6)$$

$$h(x,y) = k(x,y)h_0(o_x, o_y) \quad (7)$$

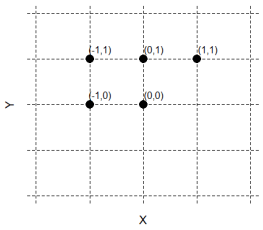

Fig. 4: State definition for 1-st order NSHP supports

The PSF $h_0(o_x, o_y)$ estimation from two consecutive images is a chellenging problem. Many previous researchers have attempted to solve this problem, including blinded and un-blinded models [22] [23]. In this paper, a weighted mean method is employed to approximate the PSF. First, a region with the same size is cropped from $g_1(x, y)$ and $g_2(x, y)$, and then the weighted kernel can be obtained in the frequency domain using

$$H = \frac{G}{F} \quad (8)$$

where F, G, and H are the Fourier Transforms of f, g, and h respectively. In this paper, considering the requirement of accuracy and complication of 3D tip localization, we proposed a UKF based model to estimate the scale factor $k(x, y)$. This model utilizes the neighbourhood pixel points, which does not require the image Jacobin matrix of a non-linear system, making the computation more efficient. Finally, the depth information corresponded to each pixel in the blurred image g can be solved using a scale factor map $k(x, y)$.

C. 2-D AR Modeling

The original blurred image structure can be represented by the random field [24] [25]. The choice of the model is a trade-off between the calculation feasibility and the accuracy of original image representation. In this paper, we propose a 2-D AR with the first order Non-Symmetric Half Plane (NSHP) support model to fully uncover the statistic characteristic of the discrete blurred image. One advantage of the recursion UKF is that delayed observations are not required. Let $k(x, y)$ represents the scale factor in the blurred image, $a(i, j)$ as the corresponding AR model coefficients, and $f(x, y)$ as the original image, as shown in Fig. 4. Then the image can be modeled as

$$f = A * f + e \quad (9)$$

The image model coefficient $a(i, j)$ can be obtained by minimizing the variance noise of the fitting error as

$$\sigma_v^2 = E[\{f(x,y) - \sum_{i,j \subseteq S_a} a(i,j)f(x-i, y-j)\}^2] \quad (10)$$

where S_a is the 1-st order NSHP supports.

The solution to equation (10), can be rearranged into the Yule-Walker equation as

$$r_{ff}(x,y) = \sum_{i,j \subseteq S_a} a(i,j) r_{ff}(x-i, y-j), \forall x,y \subseteq S_a \tag{11}$$

$$\sigma_v^2 = r_{ff}(0,0) - \sum_{i,j \subseteq S_a} a(i,j) r_{ff}(i,j) \tag{12}$$

The coefficients of $a(-1,0), a(-1,1), a(0,1), a(1,1)$ can be determined by solving the above linear equations, and the expectation value of $k(0,0)$ will be fed into the following Unscented Kalman Filter.

D. Unscented Kalman Filter

The state of depth scale factor at coordinates (x,y), denoted by $X^{(x,y)}$, contains all the pixels in a captured frame that needs to determine the future response. When the image model has a 1-st order NSHP supports, at time-step $k-1$, the states of X_{k-1} include neighbours of $X_{k-1}^{(-1,0)}, X_{k-1}^{(-1,1)}, X_{k-1}^{(0,1)}, X_{k-1}^{(1,1)}$. According to Unscented Kalman Filter theory [26], a state estimation at every time step can be obtained by following two steps of Predict and Update. The estimation $X_{k-1|k-1}$ and covariance $P_{k-1|k-1}$ are augmented with the mean and covariance of the process noise Q_k and measurement noise R_k.

Predict Step:

$$\begin{aligned}
X^a_{k-1|k-1} &= [\hat{X}^T_{k-1|k-1} E[w_K^T]]^T \\
P^a_{k-1|k-1} &= \begin{bmatrix} P_{k-1|k-1} & 0 \\ 0 & Q_k \end{bmatrix} \\
X^m_{k|k-1} &= f(X^m_{k-1|k-1}),\ m = 0 \cdots 2L \\
\hat{X}_{k|k-1} &= \sum_{m=0}^{2L} W_s^m X^m_{k|k-1} \\
P_{k|k-1} &= \sum_{m=0}^{2L} W_c^m \left\| X^m_{k|k-1} - \hat{X}_{k|k-1} \right\|^2
\end{aligned} \tag{13}$$

Update Step:

$$\begin{aligned}
X^a_{k|k-1} &= [\hat{X}^T_{k|k-1} E[v_K^T]]^T \\
P^a_{k|k-1} &= \begin{bmatrix} P_{k|k-1} & 0 \\ 0 & R_k \end{bmatrix} \\
\hat{X}_{k|k} &= \hat{X}_{k-1|k-1} + K_k(Z_k - \hat{z}_k) \\
P_{k|k} &= P_{k|k-1} - K_k P_{z_k z_k} K_k^T
\end{aligned} \tag{14}$$

where $W_s, W_c, K_k, P_{z_k z_k}$ is the weights for the state and covariance, optimal Kalman gain and measurement cross-covariance matrix, respectively. Then the updated $\hat{X}$ which is defined by the dimensions of an image is the depth scale map of the original image. Here, the $\hat{X}_{k|k}$ and $P_{k|k}$ are the updated state estimate and updated estimate covariance, respectively.

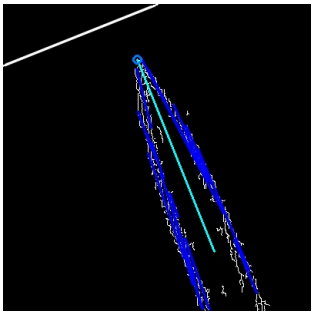

(a) Evaluation 2D coordinates

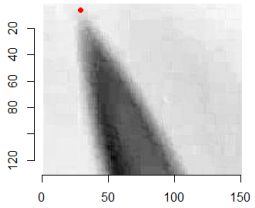

(b) Depth scale factor map

Fig. 5: Image of the tip for analysis

III. Experimental Results and Discussion

For the purpose of validation, the hardware system is first calibrated to ensure the camera is mounted up straight and parallel to the petri dish with culture medium. In the first set of experiments, the manipulator was first positioned at 19000 microns above the bottom of the petri dish and the tip was shifted upward at an increment of 1000 microns, resulting a total of 7 sets of images for analysis. The petri dish was placed on a white paper and a metal surface to examine the robustness under different backgrounds.

To alleviate the uncertainty in 2D localization as show in Fig. 5(a), a neighbourhood system is defined as

$$N = \{N_i \mid \forall_i \in S\} \tag{15}$$

where N_i is the set of neighbouring i, S is the set of lattice sites. For regular lattice image model, the neighbourhood is defined as the set of nearby sites within a radius of r

$$N_i = \left\{ i^{'} \in S | [dist(pixels_{i^{'}}, pixels_i)]^2 \leq r, i^{'} \neq i \right\} \tag{16}$$

where $dist(A,B)$ denotes the Euclidean distance between A and B. In our experiments, the r takes the value of 1.5, which 9 nearby pixels are counted as the neighbourhood. For every depth level measurement, the summation of the neighbourhood is computed, and then the mean of all 9 pixels, $\overline{x}$ column of the table I, is attained. The average scale factor value of the neighbourhood will be the estimated tip scale factor.

Table I gives the experiment results, which intuitively gives a gradual decreasing relationship between the depth and scale factor. Based on the data, the conversion from the scale factor to the actual depth in the experiment can be related by a quadratic equation. As shown in Fig. 6, the fitted equation for the two surfaces are evaluated as $y = 2.25 + 0.00924x - 0.00219x^2$ and $y = 10.4 - 0.758x + 0.0157x^2$. The non-linear relationship from the data can justify our initial choice of Unscented Kalman over other estimation methods. Also, the results indicate that there is a proportional decreasing relationship between the scale factor and the depth for a large range, especially in the range between 19000 μm to 25000 μm examined. Considering a normal cell pattern with a size between 50 μm and 100 μm [27], an operating range of 5000 μm in the out-of-plane direction will be suitable for

TABLE I: Results of Experiment I
(Subtable (a) (b) AR coefficients, corresponding to $a(-1,1), a(0,1), a(1,1), a(-1,0)$)

(a) Background of Metal Surface

Tip Position (μm)	AR Coefficients	2D X,Y Coordinates	Scale Factor $\overline{x}$	Predicted Depth Z (mm)
19000	0.2284, 0.1917, 0.3134, 0.2660	(97,71)	1.588	19.643
20000	0.2284, 0.1918, 0.3132, 0.2659	(93,63)	1.670	18.112
21000	0.2295, 0.1936, 0.3103, 0.2660	(120,79)	1.415	21.983
22000	0.2290, 0.1927, 0.3118, 0.2660	(122,62)	1.382	22.362
23000	0.2275, 0.1883, 0.3157, 0.2679	(161,49)	1.281	23.414
24000	0.2280, 0.1894, 0.3143, 0.2678	(164,51)	1.246	23.754
25000	0.2274, 0.1880, 0.3161, 0.2680	(160,50)	1.101	25.057

(b) Background of White Paper

Tip Position (μm)	AR Coefficients	2D X,Y Coordinates	Scale Factor $\overline{x}$	Predicted Depth Z (mm)
19000	0.2275, 0.1878, 0.3159, 0.2683	(85,165)	1.693	18.769
20000	0.2277, 0.1882, 0.3154, 0.2683	(91,163)	1.561	19.676
21000	0.2286, 0.1904, 0.3126, 0.2680	(108,182)	1.392	21.242
22000	0.2287, 0.1908, 0.3123, 0.2678	(100,108)	1.371	21.499
23000	0.2362, 0.2137, 0.2891, 0.2606	(107,125)	1.313	22.423
24000	0.2268, 0.1862, 0.3178, 0.2688	(106,119)	1.288	23.062
25000	0.2268, 0.1858, 0.3179, 0.2690	(110,121)	1.293	22.906

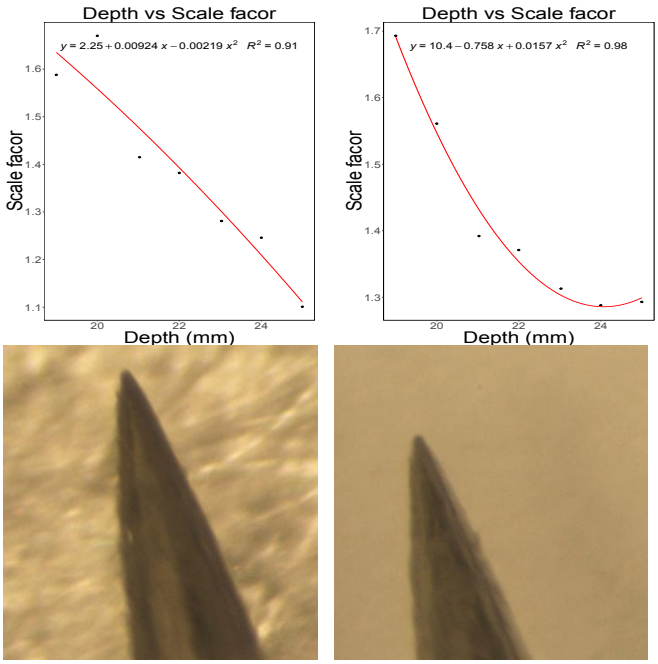

(a) Metal Surface (b) White Paper

Fig. 6: Experimental results on the correlation between scale factor and depth

the intended application and others [28] [29], where the tip position can be evaluated using the proposed method.

Comparing with the metal surface background, the results from the white paper background suffer more errors and deviate from the ground truth depth value, especially at the depth level 24000 μm. The reason is mainly due to the fact that the white paper background has a low surface roughness with little or no feature for representative analysis. In other word, the background image is sensitive to the accuracy of the evaluation method. For the image with higher contrast and resolution, the object edge and feature details are easier to be recovered. The probe tip edge on the metal surface background is much more clear, as shown in Fig. 6 (a) and (b). Any uncertainty of the tip 2D coordinates will eventually lead to the error in evaluating the depth information.

Continuous localization of the manipulator tip is another basic requirement, especially in the process of touching and poking operations. Every mistake will damage the tissue functionality or even cause damage to the probe. In the second experiment, we conduct tests to validate the precision of our algorithm. Similar to the previous experiments, the probe was moved to different depth levels and the depth scale factor of the end tip was evaluated accordingly. A total of 9 consecutive images were captured for analysis. Similarly, the influence of different background materials to the robustness of the algorithm was also examined.

From Fig. 7, we can notice a consistent result as compared with the previous experiment. There exhibits a gradual decrease relationship between the depth and the scale factor. When driving the probe upward, the detected scale factor of the end tip is increasing and vice versa. The relationship is true for both under the background colour of the metal surface and the white paper. Also, we can notice that the variation of the depth scale factor is relatively small. For example, when the probe is stationary at the depth level of 20000 μm on the metal surface, the mean depth scale factor of the tip $\overline{x}$ is 1.584, and the corresponding normalized standard deviation is 0.475. Hence, the proposed method is stable over time.

IV. Conclusion

In this paper, we propose a recursive approach to detect the 2D tip location and its depth under the cell culture medium. To account for the blurring effect caused by ripple, a motion blur model is constructed and estimated using consecutive frames. The depth scale map in the motion blur kernel was estimated using an AR model and a UKF model, and the proposed framework is proven to be efficient and robust through experiments. This method not only can apply for 3D assembly of cell sheets with a manipulator, but also gives solutions to other object manipulation tasks in water in which

TABLE II: Results of Experiment II

(a) Metal Surface

Tip position (μm)	$\overline{x}$	σ	Predicted depth Z (mm)
20000	1.584	0.475%	20.128
22000	1.462	0.589%	21.827
24000	1.232	1.235%	24.296

(b) White Paper

Tip position (μm)	$\overline{x}$	σ	Predicted depth Z (mm)
20000	1.531	0.625%	19.911
22000	1.313	0.685%	22.424
24000	1.281	0.774%	23.339

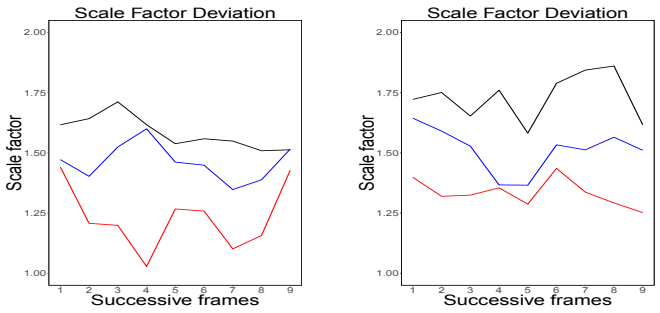

(a) Metal Surface (b) White Paper

Fig. 7: Variations on the Scale factor between successive frames

accurate 3D coordinates are needed.

REFERENCES

[1] H. Chu, Z. Huan, J. Mills, J. Yang, and D. Sun, "Three-dimensional cell manipulation and patterning using dielectrophoresis via a multi-layer scaffold structure," *Lab on a Chip*, vol. 15, no. 3, pp. 920–930, 2015.

[2] T. Masuda, N. Takei, T. Nakano, T. Anada, O. Suzuki, and F. Arai, "A microfabricated platform to form three-dimensional toroidal multicellular aggregate," *Biomedical microdevices*, vol. 14, no. 6, pp. 1085–1093, 2012.

[3] T. Anada, T. Masuda, Y. Honda, J. Fukuda, F. Arai, T. Fukuda, and O. Suzuki, "Three-dimensional cell culture device utilizing thin membrane deformation by decompression," *Sensors and Actuators B: Chemical*, vol. 147, no. 1, pp. 376–379, 2010.

[4] J. Liu, Z. Gong, K. Tang, Z. Lu, C. Ru, J. Luo, S. Xie, and Y. Sun, "Locating end-effector tips in robotic micromanipulation." *IEEE Trans. Robotics*, vol. 30, no. 1, pp. 125–130, 2014.

[5] H. Wang, Q. Huang, Q. Shi, T. Yue, S. Chen, M. Nakajima, M. Takeuchi, and T. Fukuda, "Automated assembly of vascular-like microtube with repetitive single-step contact manipulation," *IEEE Transactions on Biomedical Engineering*, vol. 62, no. 11, pp. 2620–2628, 2015.

[6] M. Schwertner, M. J. Booth, and T. Wilson, "Specimen-induced distortions in light microscopy," *Journal of microscopy*, vol. 228, no. 1, pp. 97–102, 2007.

[7] Y. Tian and S. G. Narasimhan, "Seeing through water: Image restoration using model-based tracking," in *Computer Vision, 2009 IEEE 12th International Conference on*. IEEE, 2009, pp. 2303–2310.

[8] O. Oreifej, G. Shu, T. Pace, and M. Shah, "A two-stage reconstruction approach for seeing through water," in *Computer Vision and Pattern Recognition (CVPR), 2011 IEEE Conference on*. IEEE, 2011, pp. 1153–1160.

[9] J. Konrad, M. Wang, and P. Ishwar, "2d-to-3d image conversion by learning depth from examples," in *2012 IEEE Computer Society Conference on Computer Vision and Pattern Recognition Workshops*. IEEE, 2012, pp. 16–22.

[10] W.-Y. Chen, Y.-L. Chang, S.-F. Lin, L.-F. Ding, and L.-G. Chen, "Efficient depth image based rendering with edge dependent depth filter and interpolation," in *2005 IEEE International Conference on Multimedia and Expo*. IEEE, 2005, pp. 1314–1317.

[11] S. Battiato, S. Curti, M. La Cascia, M. Tortora, and E. Scordato, "Depth map generation by image classification," in *Three-Dimensional Image Capture and Applications VI*, vol. 5302. International Society for Optics and Photonics, 2004, pp. 95–105.

[12] Y. J. Jung, A. Baik, J. Kim, and D. Park, "A novel 2d-to-3d conversion technique based on relative height-depth cue," in *Stereoscopic Displays and Applications XX*, vol. 7237. International Society for Optics and Photonics, 2009, p. 72371U.

[13] M. Gurtner and J. Zemánek, "Twin-beam real-time position estimation of micro-objects in 3d," *Measurement Science and Technology*, vol. 27, no. 12, p. 127003, 2016.

[14] S. Yuan, Z. Wang, L. Liu, N. Xi, and Y. Wang, "Stochastic approach for feature-based tip localization and planning in nanomanipulations," *IEEE Transactions on Automation Science and Engineering*, vol. 14, no. 4, pp. 1643–1654, 2017.

[15] M. Kaya, E. Senel, A. Ahmad, O. Orhan, and O. Bebek, "Real-time needle tip localization in 2d ultrasound images for robotic biopsies," in *Advanced Robotics (ICAR), 2015 International Conference on*. IEEE, 2015, pp. 47–52.

[16] Z. Ni, A. Bolopion, J. Agnus, R. Benosman, and S. Régnier, "Asynchronous event-based visual shape tracking for stable haptic feedback in microrobotics," *IEEE Transactions on Robotics*, vol. 28, no. 5, p. 1081, 2012.

[17] S. Park and W. K. Chung, "Localizing a needle tip using 2d microscope images and detecting vertical approach of a needle based on focus measures for intracellular microneedle insertion," in *Intelligent Robots and Systems (IROS), 2016 IEEE/RSJ International Conference on*. IEEE, 2016, pp. 2567–2571.

[18] S. Pertuz, D. Puig, and M. A. Garcia, "Analysis of focus measure operators for shape-from-focus," *Pattern Recognition*, vol. 46, no. 5, pp. 1415–1432, 2013.

[19] K. Seemakurthy and A. N. Rajagopalan, "Deskewing of underwater images," *IEEE Transactions on Image Processing*, vol. 24, no. 3, pp. 1046–1059, 2015.

[20] M. Sorel and J. Flusser, "Space-variant restoration of images degraded by camera motion blur," *IEEE Transactions on Image Processing*, vol. 17, no. 2, pp. 105–116, 2008.

[21] C. Paramanand and A. N. Rajagopalan, "Depth from motion and optical blur with an unscented kalman filter," *IEEE Trans Image Process*, vol. 21, no. 5, pp. 2798–811, 2012.

[22] A. Levin, "Blind motion deblurring using image statistics," in *Advances in Neural Information Processing Systems*, 2007, pp. 841–848.

[23] J. H. Elder and S. W. Zucker, "Scale space localization, blur, and contour-based image coding," in *Computer Vision and Pattern Recognition, 1996. Proceedings CVPR'96, 1996 IEEE Computer Society Conference on*. IEEE, 1996, pp. 27–34.

[24] R. C. Dubes and A. K. Jain, "Random field models in image analysis," *Journal of applied statistics*, vol. 20, no. 5-6, pp. 121–154, 1993.

[25] S. Valteris, "Autoregressive models of 2d random fields," *Informatica*, vol. 5, no. 1-2, pp. 231–240, 1994.

[26] S. J. Julier and J. K. Uhlmann, "New extension of the kalman filter to nonlinear systems," in *Signal processing, sensor fusion, and target recognition VI*, vol. 3068. International Society for Optics and Photonics, 1997, pp. 182–194.

[27] K. Huang, H. K. Chu, B. Lu, and L. Cheng, "Characterization of a Microchip Device for Cell Patterning via Negative Dielectrophoresis," in *2018 IEEE International Conference on Robotics and Biomimetics (ROBIO)*. IEEE, 2018, pp. 1521–1526.

[28] G. Marani, S. K. Choi, and J. Yuh, "Underwater autonomous manipulation for intervention missions auvs," *Ocean Engineering*, vol. 36, no. 1, pp. 15–23, 2009.

[29] M. Prats, J. C. Garcia, J. J. Fernandez, R. Marin, and P. J. Sanz, "Advances in the specification and execution of underwater autonomous manipulation tasks," in *OCEANS 2011 IEEE-Spain*. IEEE, 2011, pp. 1–5.